NANO · MICRO small
www.small-journal.com

Exploring the Charge Storage Dynamics in Donor–Acceptor Covalent Organic Frameworks Based Supercapacitors by Employing Ionic Liquid Electrolyte

*Amrita Chatterjee, Jiamin Sun, Kuber Singh Rawat, Veronique Van Speybroeck, and Pascal Van Der Voort**

Two donor–acceptor type tetrathiafulvalene (TTF)-based covalent organic frameworks (COFs) are investigated as electrodes for symmetric supercapacitors in different electrolytes, to understand the charge storage and dynamics in 2D COFs. Till-date, most COFs are investigated as Faradic redox pseudocapacitors in aqueous electrolytes. For the first time, it is tried to enhance the electrochemical performance and stability of pristine COF-based supercapacitors by operating them in the non-Faradaic electrochemically double layer capacitance region. It is found that the charge storage mechanism of ionic liquid (IL) electrolyte based supercapacitors is dependent on the micropore size and surface charge density of the donor–acceptor COFs. The surface charge density alters due to the different electron acceptor building blocks, which in turn influences the dense packing of the IL near its pore. The micropores induce pore confinement of IL in the COFs by partial breaking of coulomb ordering and rearranging it. The combination of these two factors enhance the charge storage in the highly microporous COFs. The density functional theory calculations support the same. At 1 A g^{-1}, TTF-porphyrin COF provides capacitance of 42, 70, and 130 F g^{-1} in aqueous, organic, and IL electrolyte respectively. TTF-diamine COF shows a similar trend with 100 F g^{-1} capacitance in IL.

1. Introduction

Recent years have seen a dramatic increase in the understanding and subsequent applications of supercapacitors as energy storage devices that can deliver high power density and long life cycles. Depending on the energy storage mechanism and properties of electrode materials, supercapacitors can be subdivided into a) electrical double-layer capacitors (EDLCs) and b) pseudocapacitors. In EDLCs, the electrical energy is stored via non-Faradaic processes of adsorption of ions on the electrode surface (also called electrosorption), thus involving no electron transfer between the electrolyte and electrode. On the other hand, pseudocapacitors store energy by non-Faradaic redox chemical processes, where interfacial electron transfer occurs between the electrolyte and electrode. The purely electrostatic mechanism makes EDLCs possess better power density and life cycles compared to pseudocapacitors and batteries, where short term instantaneous power supply is required.[1,2] The instantaneous polarization that occurs at electrode/electrolyte interface in EDLCs demands materials with high surface area and electrical conductivity. However, due to practical aspects, such high surface area is not easy to maintain and sustain, leading to poor energy density in EDLCs.[3,4] Currently, EDLCs using porous carbons as electrode materials dominate the market, providing high power density but limited energy density of <10 Wh kg^{-1}.[5]

The most popular materials for EDLCs constitute carbon and its variations such as carbon nanotubes (CNTs), graphene, and carbide derived carbons. Covalent organic frameworks (COFs) are a novel class of materials that have high surface area and ordered porosity, compared to activated carbons.[6] Conventional pristine COFs possess a high surface area (>2000 m^2 g^{-1}), yet have not been substantially explored in EDLCs, mainly due to their poor electrical conductivity. TTA–DHTA COF composed of 4,4′,4′′-(1,3,5-triazine-2,4,6-triyl)trianiline and 2,5-dihydroxyterepthaldehyde grown on amino-functionalized CNTs exhibited energy and power density of 11.33 Wh kg^{-1} and 272 W kg^{-1}, respectively.[7] However, the supercapacitor showed contributions partially from pseudocapacitance occurring at the redox active sites of the COF. Similar results were observed when vertically oriented ultrathin COF-1 nanosheets were grown on functionalized graphene oxide. Owing to their boron content, the COF-1 showed capacitance of ≈170 F g^{-1} in an aqueous electrolyte in a 3-electrode system.[8] We must note that alternating strategies like employing redox active electrolyte or

A. Chatterjee, J. Sun, P. Van Der Voort
COMOC-Centre for Ordered Materials
Organometallics and Catalysis; Department of Chemistry
University of Ghent
Krijgslaan 281 (S3), Ghent 9000, Belgium
E-mail: pascal.vandervoort@ugent.be
K. S. Rawat, V. Van Speybroeck
Center for Molecular Modeling (CMM)
Ghent University
Zwijnaarde, Ghent B-9052, Belgium
The ORCID identification number(s) for the author(s) of this article can be found under https://doi.org/10.1002/smll.202303189

DOI: 10.1002/smll.202303189

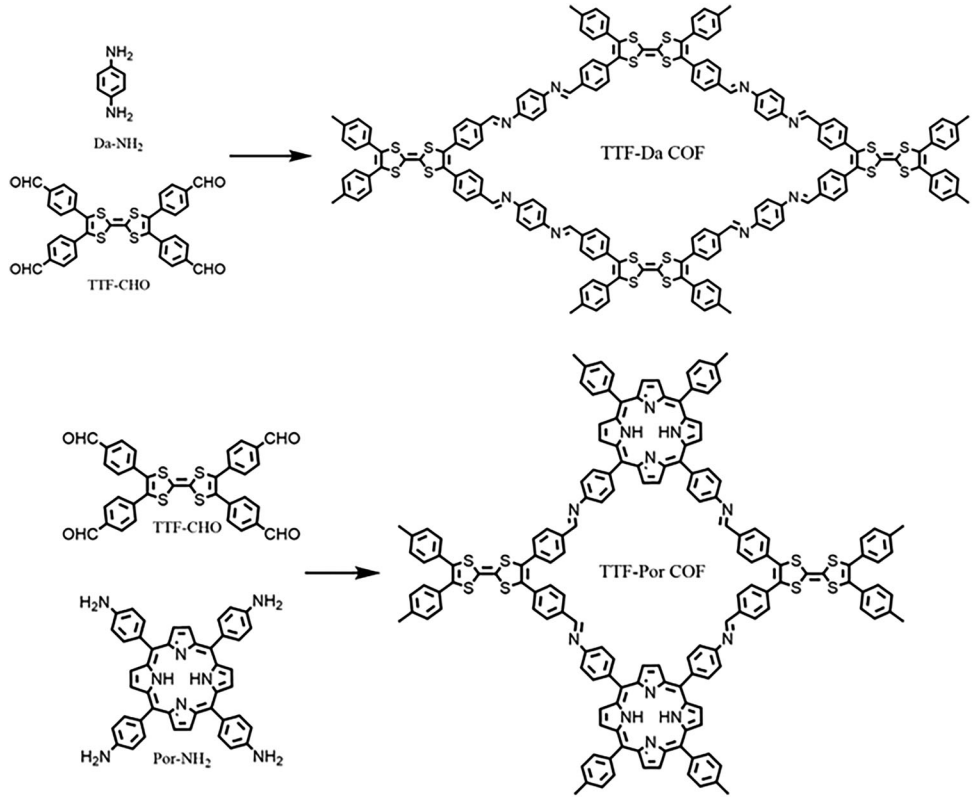

Scheme 1. Schematic of the synthesized TTF-Da COF and TTF-Por COF.

incorporating conducting polypyrrole in COF pores have also been explored to increase the performance of the COF-based supercapacitors. But these strategies typically uses pseudocapacitance and therefore are not in the scope of this work.[9,10] Till date, the only notable work on pure EDLC based on pristine COF electrodes is by Yusran et al. The exfoliated porphyrin-based JUC-511 COF achieved ideal EDLC behavior in organic electrolyte with an impressive power density of 55 kW kg^{-1}. The conductivity of the porphyrin network contributed to a low relaxation time of 121 ms, which improved the capacitive response of the supercapacitors.[11] Most COFs have been investigated as pseudocapacitors for their rich redox moieties, but the higher energy density in pseudocapacitance comes at the expense of power density and life cycle. Therefore, the role of COFs in EDLCs should be further probed to improve their energy density. Since energy density is proportional to the square of the applied voltage, therefore, a key strategy to increase the energy storage capacity of COF-based EDLCs is to utilize electrolytes with expanded electrochemical windows. This can be achieved by employing organic (2.7 V window) or room temperature ionic liquids (ILs) (4 V window) as electrolytes instead of the conventional aqueous one (0.9 V window) that have been used in COF-based supercapacitors so far. ILs are a class of low temperature molten salts that have high electrochemical stability, negligible volatility, nonflammability, low cost, and green properties. A careful choice of the anion or cation of ILs allows the modification of ionic conductivity and design of high-voltage supercapacitors.[2] Hence, they are very suitable alternatives for conventional electrolytes. Previous studies on ILs as electrolytes have mainly focused on ion-dynamics inside carbon pores and have revealed interesting phenomena.[3,12–14] For instance, changes in coordination geometry of ILs and phase changes in ILs during charge–discharge of carbon-based EDLCs are dependent on factors like pore size, crystallinity, and heteroatom doping. However, to understand such structure-property relationships of these complicated phenomena of electro-sorption and diffusion of electrolytes, porous carbons with disordered porosity are not good model materials. Recently, Bi et al, reported metal–organic frameworks (MOFs) as model materials to present a generic understanding of the energy storage mechanism and ion-dynamics of IL electrolytes in MOF-based EDLCs.[4] But for sustainable and light-weight energy devices, it is indeed a necessity to understand IL ion dynamics in metal-free model materials like donor–acceptor COFs. By tuning the precursors and the subsequent physical and chemical properties of COFs, it will be easy to obtain curated electrode materials for various electrolytes. To the best of our knowledge, such exploration on the role of electrolyte in COF-based supercapacitors has not been conducted yet.

It is important to keep in mind, that unlike in aqueous or organic electrolytes, the ionic coupling and ionic density in ILs are high.[15] Thus, their EDLC behavior is different from the former electrolytes where complete separation of ions dictates the thickness of EDLC. In contrast, the EDLC in IL-based supercapacitors is often dictated by the rearrangement of the electrolyte. Experimental evidence from electrochemical quartz crystal microbalance (EQCM) experiments of single layer graphene (SLG) or carbide derived carbon (CDC)-based ionic liquid EDLCs and the corresponding theory of overscreening versus overcrowding

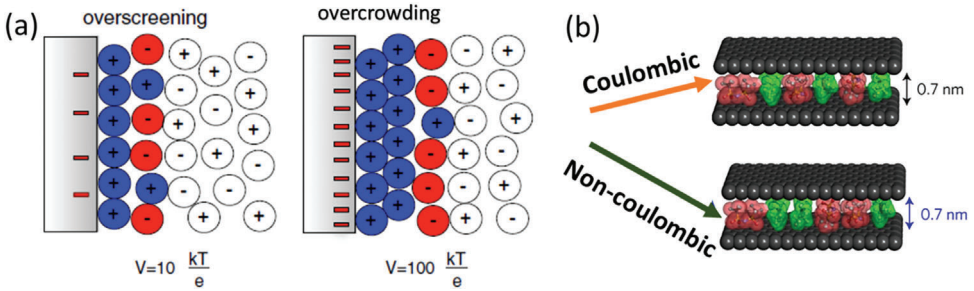

Figure 1. a) Schematic of overscreening versus overcrowding effect;[16] b) conceptual images of the structure of EMI–TFSI confined inside carbon nanopores with or without Coulombic ordering.[17] The green and red denotes the cationic and anionic part of the ionic liquid respectively.

(**Figure 1**a), postulates that at low potential the IL forms a monolayer of ions overcompensating the charge of the electrode surface. Following this monolayer, a second layer of excess counterions is formed, and such layers continue to occur till charge neutrality is achieved, consequently overscreening the electrode surface. A further increase of the potential leads to the growth of a first layer of high quantity of oppositely charged ions to the electrode thus overcrowding the electrode surface.[16]

However, such models are oversimplified and further experimental investigations have shown that understanding of the EDLC in IL electrolyte requires the consideration of the mobility difference of their cationic and anionic parts.[18] In highly porous material electrodes, the IL electrolyte functions in more complex manner. In suitable pore size, the IL supposedly encounters pore confinement followed by a phase transition. Modeling and experiments by Kiyohara and Futumura showed that microporous carbon in presence of $EMIMBF_4$ and EMIMTFSI ionic liquid electrolyte, initially undergoes monolayer confinement of counter and co-ions (Figure 1b). The charge density ramped by such monolayer confinement continues till a certain potential, after which the coulombic ordering of IL partially breaks, leading to co-ion pair formation (analogous to phase transition or rearrangement). The compensation charge induced by these non-coulombic and otherwise repulsive co-ion pairs, increases the capacitance in microporous electrodes.[17,19]

In this work, we have tried to exploit the presence and contribution of such phase transitions of IL under pore confinement in COF-based EDLCs. Hence, we focused on systematic understanding of the charge storage and transfer mechanism of two tetrathiafulvalene (TTF)-based 2D donor–acceptor COFs, with different electron acceptor groups a) *p*-phenylenediamine and b) 5,10,15,20-tetrakis (*para*-aminophenyl)–21H,23H-porphyrin (**Scheme 1**). The COFs have been used as electrodes in symmetrical supercapacitors employing different electrolytes, namely aqueous, organic, and IL to analyze the dynamics of the electrolyte ions with respect to the ordered pore structure of reticular donor–acceptor COFs and their modified electronic pathway arising from change in the electron acceptor concentration of building blocks.

Our work sheds light on the fact that apart from the pore size and crystallinity, the functionality of building blocks of the COFs tends to change the electronic polarity of the pores that influences the confinement process of ILs in the pores. Therefore, the poor electrical conductivity of COFs can be circumvented by employing matching electrolytes to enhance their energy storage capacity.

2. Results and Discussion

First of all, the TTF-COFs consist of the TTF units with strong donor property. In order to construct donor–acceptor COFs a judicious choice of donor and acceptor moieties must be made, so that their orbitals match. These TTF-COFs have been previously reported and their strong donor–acceptor properties have been measured and described previously.[20,21] Second, the poor electrical conductivity of COFs is a well-known issue that deters its wide spread application in the electrochemical energy storage field. The presence of TTF in the conjugated framework imparts electrical conductivity to the COFs.[22] Furthermore, theoretically COFs are reticular materials and can be synthesized with great tunability of monomers. However, in practice not all COFs are very easy to prepare in sufficient quantity and perfect precision. Although we were able to synthesize TTF COFs with alternative monomers, we did not reach the same comparable crystallinity and surface area as for the TTF-Por and TTF-Da COFs. Since this work focuses only on the pore confinement effect of ionic liquid EDLCs, the TTF-COFs that had similar crystallinity and surface area were selected. That way the pivotal focus lies on the effect of pore size and polarity of the pore walls on EDLC. Finally, EDLC depends on electrochemical surface area which is influenced not only by specific surface area but also by electrical conductivity, wettability, and surface roughness.[23,24] These factors modify the ion diffusion and transport properties. The TTF COFs in this work, might have slightly lower specific surface area but their content of heteroatoms and electrical conductivity influence the charge storage properties to a great extent. Striking of balance between the above mentioned factors made the TTF-COFs our model of choice to obtain high electrochemical surface area when used as EDLC devices.

Two TTF-based imine COFs were synthesized via a Schiff-base condensation reaction of TTF-CHO with 1,4-diaminobenzene (Da-NH_2) or 5,10,15,20-tetrakis (para-aminophenyl)–21H,23H-porphyrin (Por-NH_2) to obtain the corresponding TTF-Da COF and TTF-Por COF materials (Scheme 1). The crystallinity of the synthesized COFs was confirmed by powder X-ray diffraction (PXRD). As shown in **Figure 2**a,b, the synthesized TTF-Da COF and TTF-Por COF exhibit a sharp and intense diffraction peak at 4° and 5.5° (2θ) respectively, which matches well with simulated PXRD patterns obtained from the literature.[20,21] Moreover,

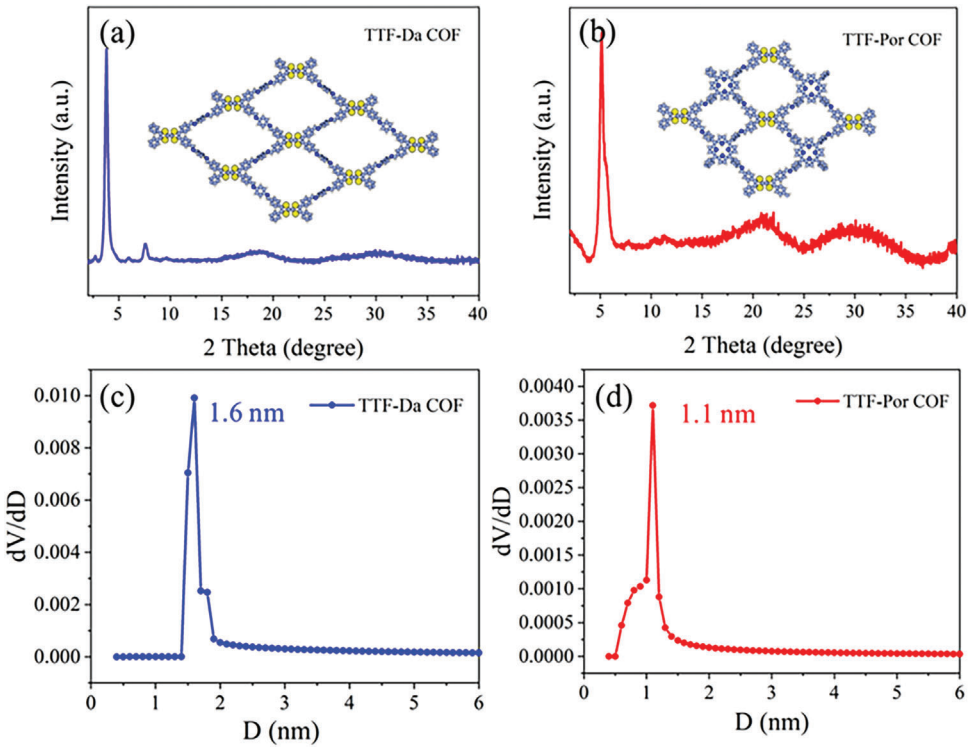

Figure 2. a,b) XRD patterns and c,d) pore size distribution of TTF-Da COF and TTF-Por COF.

according to the simulated patterns, the experimental PXRD patterns for all the synthesized TTF-COFs are consistent with the simulated eclipsed (AA) arrangement rather than staggered (AB) stacking (Figure S1, Supporting Information). To assess the textural properties of the synthesized COF materials, argon sorption measurements were performed at 87 K. As shown in Figure 2c,d and Figure S2a, Supporting Information, both TTF-Da COF and TTF-Por COF display a type I isotherm. The Brunauer–Emmett–Teller surface area and total pore volume (at $P/P_0 = 0.99$) of TTF-Da COF and TTF-Por COF are 496 $m^2\ g^{-1}$ (pore volume = 0.30 $cm^3\ g^{-1}$) and 424 $m^2\ g^{-1}$ (pore volume = 0.29 $cm^3\ g^{-1}$) respectively. The results of the pore size distribution analysis of TTF-Da COF and TTF-Por COF using argon sorption-based quenched solid density functional theory method show a distribution with a center of 1.6 and 1.1 nm respectively. The imine bond formation of the COFs was verified by Fourier transform infrared spectroscopy (FT-IR). The characteristic C═N vibration band is clearly observed at 1624 and 1627 cm^{-1} in the spectra of TTF-Da COF and TTF-Por COF, respectively (Figure S2b, Supporting Information). In contrast, the FT-IR spectra of the organic monomers Por-NH_2, Da-NH_2, and TTF-CHO do not show the imine peaks. Next, it can be seen that the intensity of the C═O vibration band (1600–500 cm^{-1}) reduces with the formation of COFs as compared to TTF-CHO indicating the consumption of aldehyde to form the imine bond in COFs. The TGA data in Figure S2c, Supporting Information, show no obvious weight loss up to ≈400 °C, corroborating the excellent thermal stability. The lower intensity of the photoluminescence spectra (Figure S2d, Supporting Information) of TTF-Por COF compared to TTF-Da COF can be attributed to the higher charge delocalization through the extensive conjugated framework of TTF-Por COF that is composed of donor and acceptor monomers with the highest difference in electronegativity. The higher amount of charge delocalization ensures lower recombination and faster electron transport. X-ray photoelectron spectroscopy analysis shows the presence of sulfur and nitrogen in the backbones of both TTF-COFs (Figures S3 and S4a–d, Supporting Information). Scanning electron microscopy (SEM) and high resolution transmission electron microscopy images displayed that TTF-Da COF and TTF-Por COF both have a flake-like morphology (Figures S5 and S6, Supporting Information). Before using the TTF-COFs as electrodes for supercapacitors, their chemical stability was tested in water, acetonitrile, and $EMIMBF_4$. The XRD patterns in Figure S7, Supporting Information, show no significant change in their crystallinity implying their safe use in the electrolytes used in this work.

The EDLC performance of the 2-electrode COF-based symmetric supercapacitor devices has been investigated in three electrolytes, namely: 1 M Na_2SO_4 in water (aqueous electrolyte), 1 M $TEABF_4$ in ACN (organic electrolyte), and $EMIMBF_4$ (IL electrolyte). The electrochemical performance has been evaluated through electrochemical impedance spectroscopy, cyclic voltammetry (CV), and galvanostatic charge–discharge (GCD). It is clear from **Figure 3**a–c that in presence of aqueous and organic electrolyte, both the TTF-Da and TTF-Por COFs showed smooth CVs. However, it is only for the IL-based devices, that both the COFs show a small peak at cell voltage of ≈1.4–1.6 V (negative polarized curve) at small scan rates and does not vanish after five cycles (Figure S8a, Supporting Information). This is contrary to redox reactions. We also ruled out that our systems are plagued by

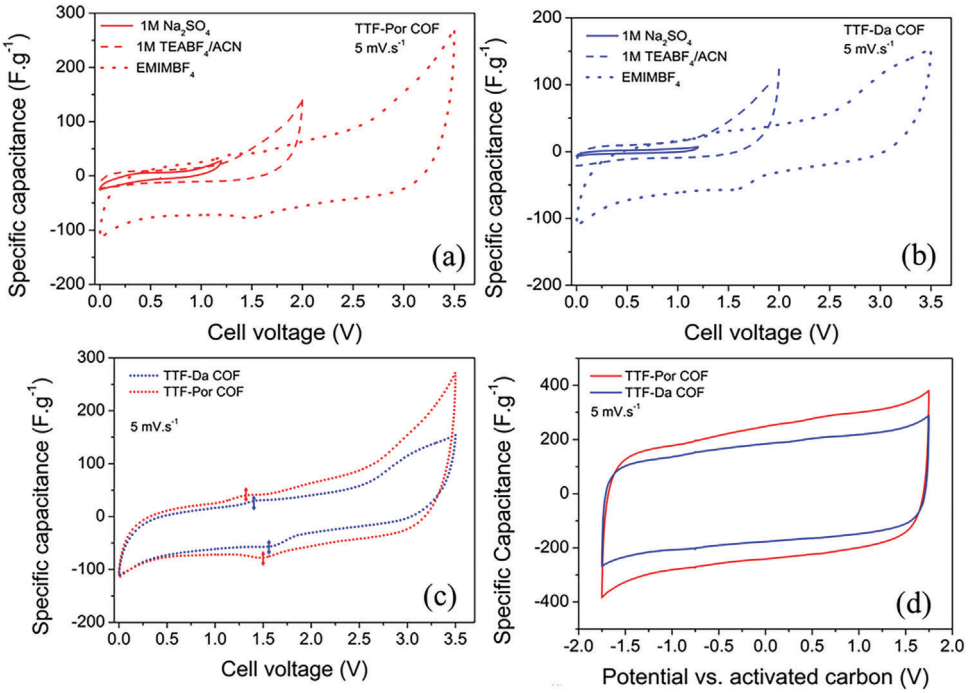

Figure 3. a) CV in 2-electrode devices for TTF-Por COF in aqueous, organic, and IL electrolyte; b) CV in 2-electrode device for TTF-Da COF in aqueous, organic, and IL electrolyte; c) CV comparison in 2-electrode device for TTF-Por COF and TTF-Da COF in IL electrolyte; and d) CV in 3-electrode configuration for TTF-Por and TTF-Da COFs in IL electrolyte.

impurities, since then such parasitic reactions would have been evidenced in the other CVs as well. But that is not the case.

To investigate if the peak was from the decomposition of IL electrolyte we conducted CV till higher voltage to confirm the potential of decomposition of IL. But it can be seen from Figure S8b,c, Supporting Information, that the IL decomposition in both TTF-Por COF and commercial activated carbon starts only after 4.8 V and due to the irreversible nature of the degradation reaction the successive peaks had lower current density. Activated carbon has been used as a control material to confirm that the peak above 4.8 V is indeed due to electrolyte decomposition and not due to material property of TTF-Por COF.

To verify the cause of the reversible peak, further analysis in 3-electrode configurations was carried out. The CVs in 3-electrode configuration depicted in Figure 3d show rectangular CVs with evidence of such peak, confirming that the IL-based devices are indeed EDLCs and the peak is caused by micropore filling/emptying mechanism. The high operating window of IL provides a higher specific capacitance for both COFs. Since the stability of aqueous and organic electrolyte is no more than ≈2 V, naturally the specific capacitance obtained was less. The higher specific capacitance of TTF-Por COF in IL compared to TTF-Da COF can be attributed to the surface charge density (arising from the stronger electron acceptor porphyrin building block) and smaller pore size for confinement effect. Since the crystallinity and surface area of the COFs are nearly similar, we rule out these possibilities as enhancement parameters. **Figure 4**a,b proves that even with increasing scan rate till 100 mV s^{-1}, the quasi-rectangular

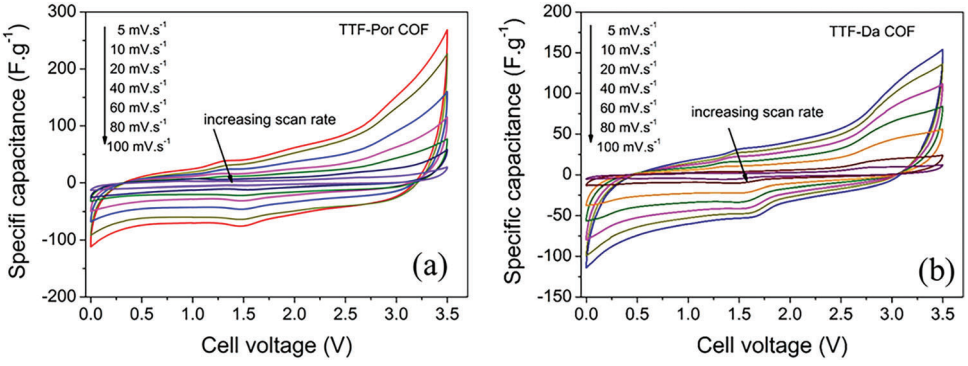

Figure 4. CV in 2-electrode devices with IL electrolyte at different scan rates for a) TTF-Por COF and b) TTF-Da COF.

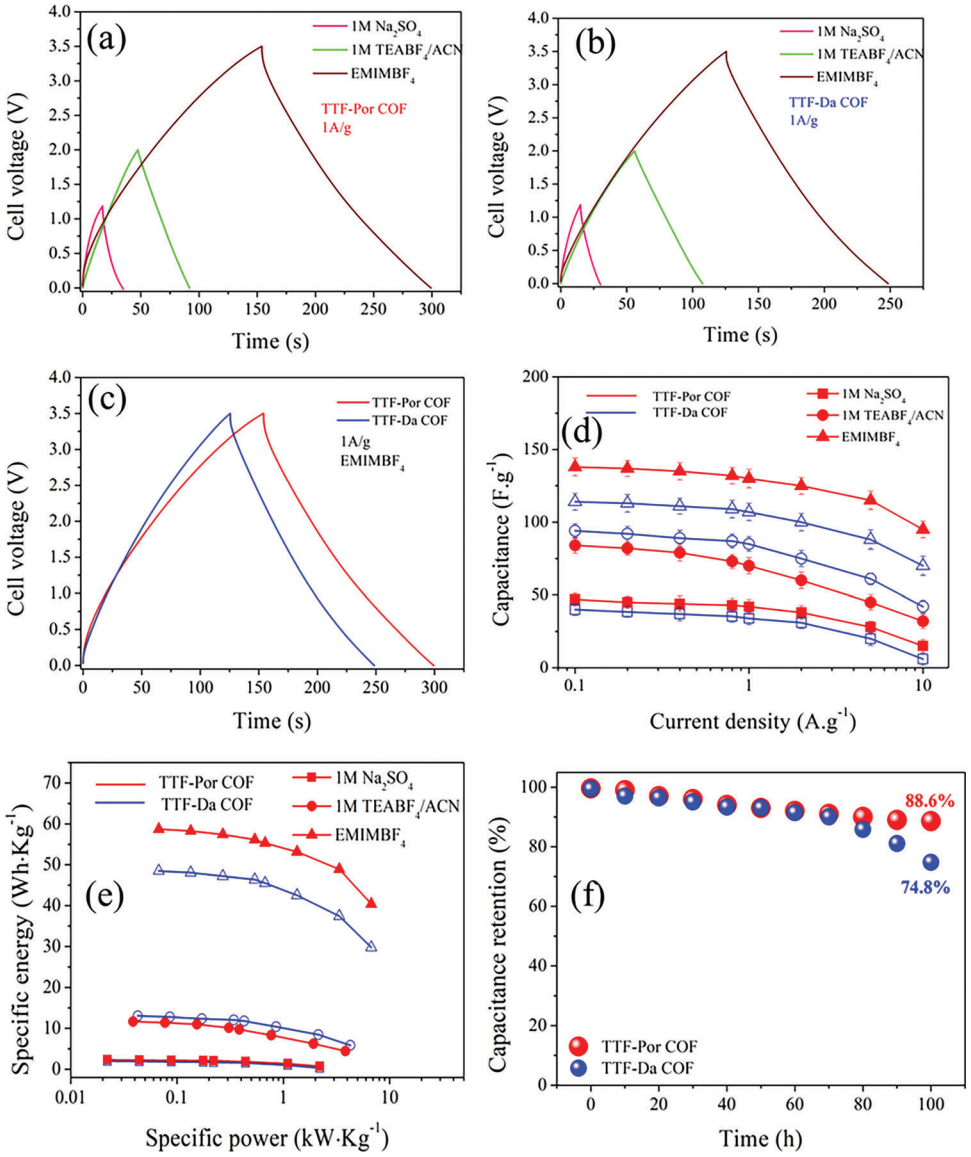

Figure 5. GCD profiles in various electrolytes for a) TTF-Da COF and b) TTF-Por COF; c) comparison of GCD profiles of TTF-Da COF and TTF-Por COF in EMIMBF4; d) specific capacity versus current density of TTF-Da and TTF-Por COF in various electrolytes; e) Ragone plot; f) stability test.

shape of CV persists without any apparent redox peaks, thus validating the superiority of the TTF-Por COF EDLC in IL. However, the anomalous peaks at 1.4–1.6 V tend to disappear with increased scan rate, due to the rapid adsorption–desorption of ions and restricted diffusion of electrolytes into the pores, resulting in a lowering probability of phase transitions of IL inside the pores, and consequently lower capacitance. The GCD profiles in **Figure 5**a–d and Figure S9a–f, Supporting Information, shows that at low specific current density of 0.1–1 A g^{-1}, the specific capacitance of TTF-Da-COF and TTF-Por-COF normally improves with the change in electrolyte as: aqueous < organic < IL. The wide voltage window is definitely one of the reasons. But it should also be noted that the increased charge difference between the electron acceptor porphyrin and electron donor TTF in TTF-Por COF improves the charge delocalization across its framework. This results in stronger electrostatic attraction between the electrolyte and the COFs at the interface and dense packing of cations inside the pores, forming a wider EDLC. The TTF-COF based EDLCs yielded results even at high current density of 10 A g^{-1}. The capacitance reduced drastically at higher current densities due to the fast charge–discharge time that directly affects the time for electrolyte ion diffusion into the pores and subsequently their charge storage capacitance. The rate capabilities of the COFs show distinct improvement in IL electrolyte as compared to in organic or aqueous electrolyte. This implies that the transport distance of ions to reach the micropores is shortened accordingly in the electrolytes, thus improving their rate capabilities. Notably, the transport distance of IL ions in TTF-Por COF is less than that in TTF-Da COF. This confirms the idea that smaller and narrower micropores improve the rate capability in COFs. It can be concluded from the Ragone plot (Figure 5e) that the energy density of the TTF-based COFs shows an increasing trend with the voltage

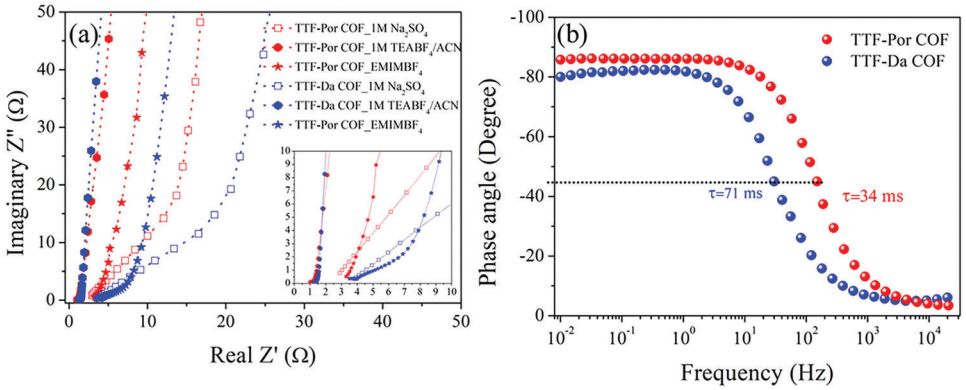

Figure 6. (Left) Nyquist plot of TTF-Por and TTF-Da COFs in various electrolytes at OCV; (right) Bode plot of TTF-Por and TTF-Da COFs in $EMIMBF_4$ at OCV.

windows of the electrolytes. In fact, the TTF-Por COF EDLC supercapacitor with ionic liquid electrolyte recorded an impressive energy density of 58 Wh kg^{-1} at 1 kW kg^{-1} power density. Even after increasing the power density to 6.7 kW $kg^{-1,}$ it could maintain a decent energy density of 40 Wh kg^{-1}. On comparing the capacitance performance of the TTF-COFs (Table S1, Supporting Information) with state of the art metal free COFs and carbon used for EDLC supercapacitors, it can be seen that this work presents till date the best power density versus energy density obtained for COF-based EDLC supercapacitors and is even comparable to the redox-type pseudocapacitors with COF electrodes.[25,26] In fact, the energy density of COF-based EDLC supercapacitors obtained from this work is almost twice higher than commercial activated carbon and mesoporous carbon.[26] It should be noticed that the energy density in the TTF-based COF supercapacitors with IL electrolyte increased approximately six times compared to organic electrolyte and ≈40 times compared to aqueous electrolyte, without compromising the power density of course. This high performance is attributed to the wide electrochemical window of ionic liquid and their phase transition in micropores. The stability of the COFs in IL electrolyte was tested by floating test method by holding the cells at 3.5 V for 100 h and cycling them at 1 A g^{-1} at every 10 h. Both COFs showed good capacitance retention of 74–88% after 100 h as shown in Figure 5f. The constriction of the electrochemical window in non-Faradaic region eliminates the redox activity of the COFs, thus improving their long term cyclic stability.

Post-GCD characterization by ATR (Figure S10, Supporting Information) of the TTF-Da and TTF-Por COF electrodes reveal no significant changes between the pristine electrode and after 80 h of GCD. The porous electrodes adsorb the $EMIMBF_4$, thus making it almost impossible to obtain the signal of imine bond of the COFs. The peaks at 2990, 1570, 1170, and 1081 cm^{-1} indicate the C—H, C═C, C—N, and BF_4 stretching vibrations of the imidazolium ring and the anion of the IL accordingly. Since, the IL adsorbed pristine electrodes show almost similar spectra to the one after 80 h of GCD, it can be concluded that no chemical interaction has happened during the cycling in the device. In other words, the COF-based EDLC device operates by physical sorption of ionic liquid ions.[27–29] Similarly the SEM images in Figure S11, Supporting Information, also show no significant morphological changes before and after 80 h of GCD.

The Nyquist plots in **Figure 6**a have been measured at open circuit potential (OCV) of the 2-electrode devices. All the plots have depressed semicircle and nearly linear region at low frequency in both of TTF-Da and TTF-Por COF-based supercapacitors in all three electrolytes, indicating near-ideal capacitive behavior of the cells. The slight deviation from vertical slope is due to the slow transport of the viscous $EMIMBF_4$ electrolyte within the COF pores. The corresponding Bode plot of the TTF-COFs in ionic liquid electrolyte in Figure 6b shows that at high frequency, the phase angle is ≈0. But with frequency decreasing to below 100 Hz, the phase angle rapidly rises and reaches a limitation at approximately −90°, which indicates the closer approximation to ideal capacitor. Further comparison can be done of the characteristic frequency f_0 at which the phase angle corresponds to 45°. The corresponding relaxation time τ_0 ($\tau_0 = 1/f_0$) signifies the minimum time needed for complete discharge of the device with greater than 50% efficiency.[30] The lower time constant of 34 ms in TTF-Por COF EDLC supercapacitor points toward faster ion diffusion across the electrode/electrolyte interface and their transport within the ordered micropores of the COFs. Consequently, the TTF-Por COF supercapacitor underwent faster discharge/charging reversible cycles and contributed to the enhanced capacity retention.

To understand the electrode–electrolyte interfacial dynamics, the impedance spectra were modeled using a modified Randle's circuit that is deemed appropriate for IL double-layer capacitance. The equivalent circuit is modeled on the Nyquist plots as shown in Table S2, Supporting Information. The equivalent circuit consists of the R_s (bulk electrolyte resistance originating from the ionic conductivity of the electrolyte and electrode), R_L (leakage resistance between electrode and electrolyte ions due to dissipative reactions), CPE_{EDLC} (constant phase element indicating the double layer capacitance in porous electrode), and W_o (Warburg impedance originating due to diffusion of the electrolyte ions into the pores of electrode). Focusing on the equivalent circuit parameters of the COF electrodes in $EMIMBF_4$, we see low value of R_s in TTF-Por COF compared to TTF-Da, indicating the faster charge conduction of the electrolyte ions across the conjugated framework of TTF-Por COF. The high crystallinity of the COFs allows facile transmission of the electrolyte ions, indicating their improved electrical conductivity. Additionally, the negative surface charge of TTF-Por COF favors higher adsorption of

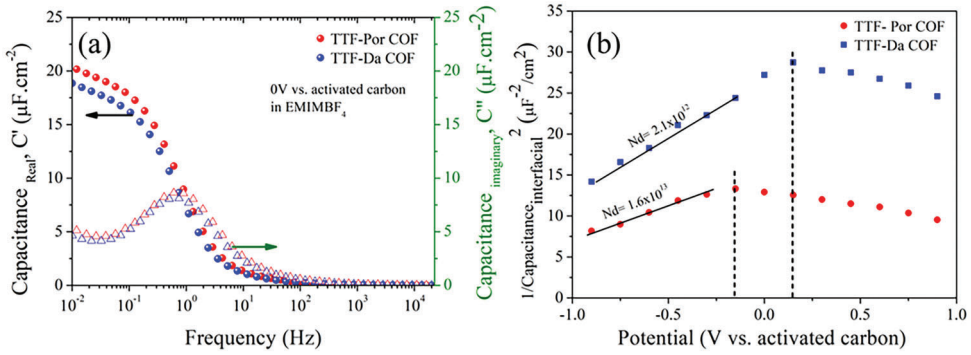

Figure 7. a) Real and imaginary parts of electrochemical capacitance of TTF-Por and TTF-Da COF measured at 0 V versus activated carbon in $EMIMBF_4$; b) interfacial capacitance versus potential curve in $EMIMBF_4$.

cationic part of IL and their subsequent confinement. The higher CPE_{EDLC} of TTF-Por COF means that higher charge storage capacitance is obtained at the interface of TTF-Por COF electrode and the $EMIMBF_4$ electrolyte. This also corroborates to the previous cyclic voltammetry. But the CPE_{EDLC} of both COF electrodes varies as Na_2SO_4/H_2O < $TEABF_4$/ACN < $EMIMBF_4$, confirming that IL electrolytes improve the capacitance to a great extent as compared to aqueous and organic electrolytes. On comparison of the Warburg impedance, a steeper slope is observed in the case of organic electrolyte compared to IL. This is attributed to the due to the partial restriction imposed by the microporous COFs on the larger size and higher viscosity of the IL. Considering the largest dimension, the size of TEA^+, ACN, $EMIM^+$, and BF_4^- are 0.67, 0.65, 0.95, and 0.51 nm, respectively.[31] In absence of a solvation shell, the neat ILs can be accommodated within the 1.1 and 1.6 nm pores of TTF-Por and TTF-Da COFs, respectively. However, the size of $EMIM^+$ is still greater than TEA^+/ACN. That explains the flatter slope and greater impedance of $EMIMBF_4$ toward ion diffusion. In principle, the lower Warburg impedance of TTF-Por COF in $TEABF_4$/ACN than $EMIMBF_4$ should imply a shorter transport distance of organic electrolyte to reach the electrode interface, thus resulting in better rate capability. But GCD profiles have proven that it is in ionic liquid electrolyte, that both COFs show better rate capability. Therefore, we cannot rule out the possibility that the flatter Warburg impedance slope in $EMIMBF_4$ might also be an indication that pure capacitance is not the only process that occurred, but it is accompanied by complex rearrangement or phase transition of IL electrolyte within the pores.

To delve into the underlying mechanism of the superior performance of IL-based COF EDLCs, a 3-electrode configuration experiment was conducted. As mentioned previously, when CV was executed in a 3-electrode configuration, no peaks were observed, confirming the EDLC behavior of both COFs in IL electrolyte. Therefore, the increased capacitance can safely be assumed to be arising from the interactions of the ionic liquid with the polarized surface of the COFs and the subsequent rearrangement of IL electrolyte at the pore interface. To obtain the interfacial capacitance and its behavior in TTF-based ionic liquid supercapacitors, impedance spectra at various potentials were recorded.[32,33] Thereby, normalized real capacitance (C′) and imaginary capacitance (C″) of TTF-Por and TTF-Da COFs were obtained as shown in **Figure 7**a. The real capacitance accounts for the interfacial capacitance and the imaginary one corresponds to the dissipative or leakage capacitance. On processing this data, it was inferred that the interfacial capacitance of TTF-based COFs in ionic liquid is potential-dependent (Figure 7b). In other words, the interfacial capacitance is governed not only by the nature or electrodes but also by the polarization effect of the electrolyte on the electrode surface. This is true especially in concentrated electrolytes with high ion packing like ionic liquid. In such cases the interfacial capacitance is very sensitive not only to the electronic structure of the electrode material, but also to the nature of the electrolytes at the polarized interface.[32,34] The TTF-Por COF showed higher interfacial capacitance than TTF-Da COF under same conditions due to the faster rearrangement of higher content of cations/anions of IL electrolyte at the highly polarized interface of TTF-Por COF.

Before understanding the rearrangement process, let us take a look at the surface potential of the COFs, which can provide a rough estimation of the surface charge density of the polarized COF in contact with the IL electrolyte. The surface potential can be derived from the potential of zero charge (PZC). PZC is the potential where the net surface charge of electrode is zero. It roughly implies the point of minimum capacitance on the CVs, meaning that at PZC the charge starts to origin, before they are subjected to external potential.[35] Interestingly, the PZC of TTF-Por COF in IL-based supercapacitor was at −0.12 V versus activated carbon, while that of TTF-Da was at 0.09 V versus activated carbon. The more negative PZC of TTF-Por arises from the nitrogen-rich porphyrin units that decorate its pore walls. In presence of IL electrolyte, this negative surface charge of TTF-Por forces the $EMIM^+$ chain to undergo strong π–π interaction with their pore walls. On the other hand, the positive shift in PZC for TTF-Da is attributed to the change in interactions of $EMIM^+$ cations with the less negative surface charge density of TTF-Da owing to their diamine units.[32,33] Previous experiments and simulation models on interaction of ILs with SLG, CDC, and CNTs have shown similar interaction effects.[32,33,35,36] Further polarization toward negative end causes an n-type positive slope due to the increased interactions of the COFs and $EMIM^+$. The positive slope of TTF-Por COF is flatter than TTF-Da, demonstrating that the former has one order of magnitude higher charge carrier density at interface than the latter. The excess amount of charge carrier density in TTF-Por COF occurs due to its high surface charge density that enhances the screening length of the electrolyte ions,

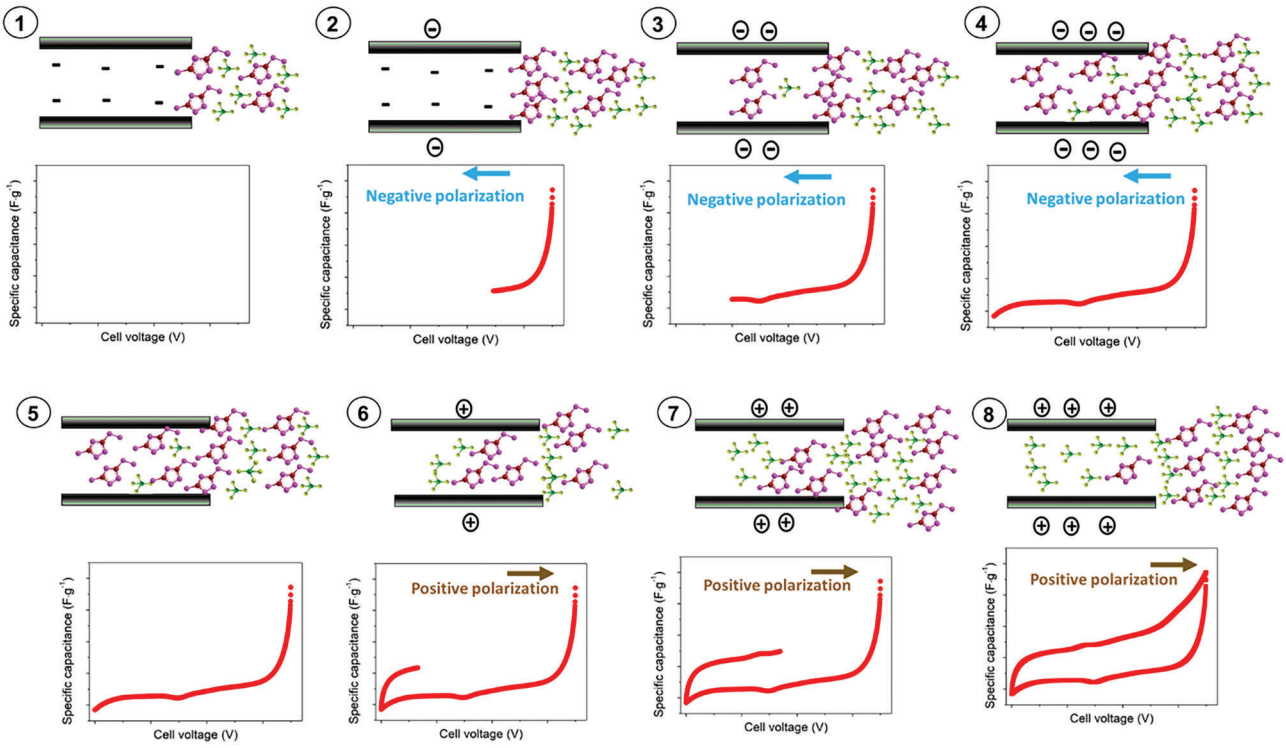

Figure 8. Mechanism of ionic liquid rearrangement in micropores of TTF-Por COF based EDLC supercapacitors. The inner walls of pores in COF have negative polarity. On applying external negative potential, the cationic $EMIM^+$ starts getting attracted toward the pores. Higher surface charge density of TTF-Por COF allows a high amount of $EMIM^+$ to come toward the pores. Further negative potential causes columbic order breaking, resulting in confinement of $EMIM^+$ in pores (cause of anomalous peak). Upon positive potential, the $EMIM^+$ gets out from pores, and BF_4^- confines inside pores. But the sluggish mobility of $EMIM^+$ compared to BF_4^-, causes unusual charge accumulation inside pores that causes the second peak. Further increase in positive potential empties the pores of $EMIM^+$ and fills them with BF_4^-.

consequently resulting in higher amount of $EMIM^+$ to be electrostatically confined in the pore walls of TTF-Por electrode compared to TTF-Da.

Combining the above analyses and density functional theory (DFT) calculations (in next section), charge storage mechanism in TTF-COF based IL supercapacitors can be viewed as in **Figure 8**. In absence of any externally applied potential, coulombically ordered IL exists in bulk such that each ion is surrounded by a shell of counterion (1). On application of potential, the ILs accumulate on the external surface, thus wetting the external surface of the pore, but do not enter the micropore yet (2). Subsequently, a certain potential is reached that can overcome the attractive forces between the counterions, partially breaking the coulombic ordering and de-coordinating them. This disruption of the energetically unfavorable breaking of coulombic ordering, forces the electrolyte ions to enter the micropores whose charge is then compensated by the pore walls (3). This combined energy transition caused by the de-coordination of IL and increased surface charge density is translated in form of the peak in the CV curve.[37] Since TTF-Por COF has higher negative surface charge density as proved from PZC, higher amount of $EMIM^+$ accumulates near its pore due to longer screening, followed by BF_4^-. Upon a negative polarization, the columbic ordering breaks, and the $EMIM^+$ gets confined into the micropores by electrostatically adsorbing on the pore walls, thus giving rise to the peak at 1.47 V in CV of TTF-Por COF. Due to the higher polarity of the pores in TTF-Por COF, dense packing of $EMIM^+$ can be obtained and hence higher accumulation of charge density. This explains the stronger peak at 1.47 V in TTF-Por COF device, compared to the peak at 1.53 V in TTF-Da, since less amount of $EMIM^+$ is confined in the latter. The EDLC formation continues till the end of negative polarization (4). Upon positive polarization, the excess adsorbed $EMIM^+$ from pores gets expelled, while BF_4^- occupies that place (5). But due to the lower mobility of $EMIM^+$ compared to BF_4^- and the negative surface charge density of the TTF-Por COF pore, all the cations cannot get desorbed (6 – 7). This leads to a charge overcompensation by the anion exchange at low voltages, leading to an unusual increase in capacitance at the positive polarization.[38] The difference in the desorption kinetics gives rise to a hysteresis that causes the second peak to appear slightly more positive 1.33 V in TTF-Por COF (8). The absence of such anomalous energy behaviors in aqueous and organic electrolytes results in their low charge storage and capacitance. For example, in the $TEABF_4$/ACN organic electrolyte, TEA^+ has smaller dimension than $EMIM^+$. So, it is natural to assume that $TEABF_4$ will enter the micropores preferably than $EMIMBF_4$. However, the capacitance performance shows otherwise. Since TEA^+ has smaller size than $EMIM^+$, therefore ionic interaction between TEA^+ and $BF4^-$ coordination shell is stronger than in $EMIMBF_4$. Therefore, the confinement of $TEABF_4$ in micropores is hindered. Additionally, $EMIM^+$ also has an added advantage of flexible structure than the rigid TEA^+, which favors it to penetrate

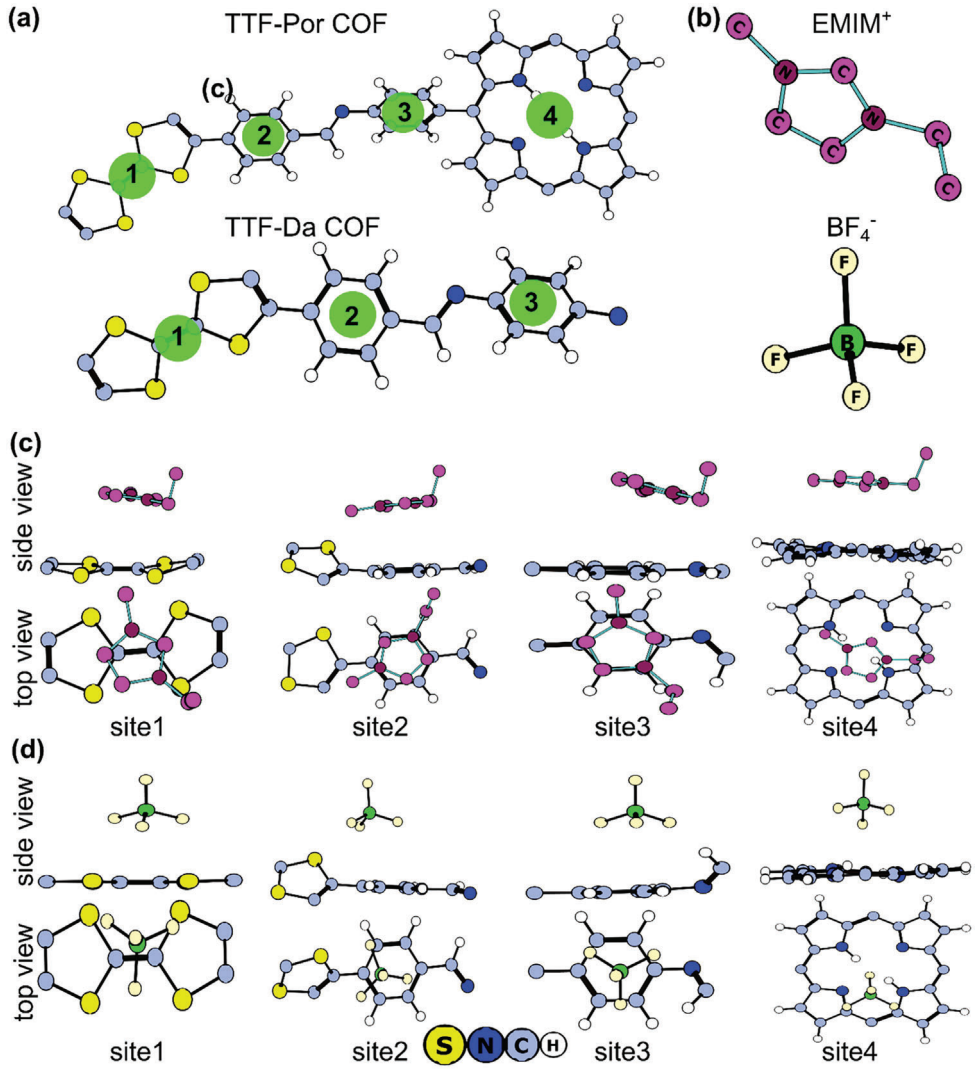

Figure 9. a) All considered adsorption sites on TTF-Por COF and TTF-Da COF; b) optimized geometries of $EMIM^+$ and BF_4^-; Optimized geometries of adsorbed c) $EMIM^+$ and d) BF_4^- on all the sites of TTF-Por COF (viewed from either the side or the top). The atom colors for COF are elaborated in the figure. H atoms of $EMIM^+$ were omitted for clarity.

the micropores during partial coulomb breaking.[36] Further investigations with EQCM[38] and in situ STM[39] would be useful to identify the species in the above mechanism.

To further understand how the electron-acceptor building block influences the surface charge density of TTF-Por and TTF-Da COFs and their effect on the charge storage mechanism in an ionic liquid electrolyte, DFT calculations were executed. All calculations were executed at the PBE-D3 (BJ)[40–42] level as implemented in the VASP package[43,44] (more details are given in the Supporting Information). The binding behavior of $EMIM^+$ and BF_4^- on TTF-based COFs was investigated at the potential distinct sites governed by functional groups of COFs (**Figure 9** and Figures S12–S14, Supporting Information). Our calculation suggests that the $EMIM^+$ preferably binds strongly at the top of the porphyrin ring (site 4) in TTF-Por COF and benzene group (site 2) in TTF-Da COF with respective adsorption energies of −1.66 and −1.40 eV (**Table 1**). This relatively stronger interaction of $EMIM^+$ with TTF-Por COF than TTF-Da COF agrees well with our experimental results. For BF_4^-, site 1 was identified as a favorable adsorption site on both COFs, with TTF-Da COF furnishing stronger adsorption (−3.94 eV) than TTF-Por COF (−3.84 eV).

Table 1. Adsorption energies (eV) of $EMIM^+$ and BF_4^- on different sites of TTF-Da COF and TTF-Por COF.

Adsorption sites	TTF-Da COF		TTF-Por COF	
	$EMIM^+$	BF_4^-	$EMIM^+$	BF_4^-
1	−1.26	−3.94	−1.40	−3.85
2	−1.40	−3.62	−1.31	−3.55
3	−1.27	−3.18	−1.19	−3.24
4	—	—	−1.66	−3.15

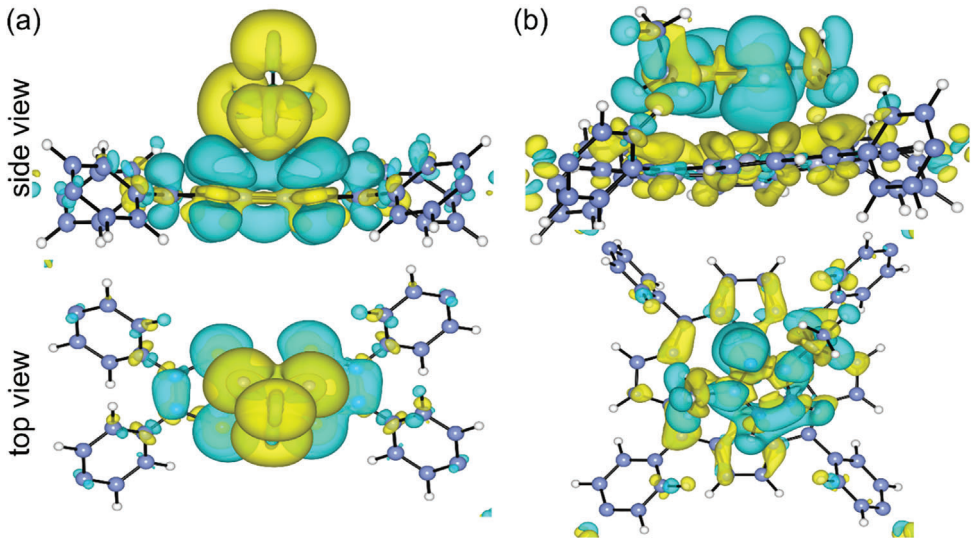

Figure 10. Charge density difference of a) adsorbed BF_4^- (site 1) and b) $EMIM^+$ (site 4) on TTF-Por COF. The cyan and yellow isosurfaces (0.001 $eÅ^{-3}$) represent the charge depletion and accumulation, respectively.

Next, the charge distribution of adsorbed structures was examined. In the case of on BF_4^- anion, the calculated charge density difference shows the charge accumulation (yellow isosurface) around BF_4^- and charge depletion (cyan isosurface) on the COF surfaces (**Figure 10** and Figure S15, Supporting Information). In contrary, charge accumulation occurs on the COF surface and charge depletion on adsorbed $EMIM^+$. This suggests that negatively charged COF surfaces provide a preferable condition for $EMIM^+$ cation to adsorb. However, the binding strength depends on the extent of charge transfer between COF and $EMIM^+$ cation. The Bader charge analysis reveals that ≈0.81 $|e|$ charge gets transferred between TTF-Por COF and $EMIM^+$ and it decreases to ≈0.72 $|e|$ for TTF-Da COF. This is in agreement with experimental results and adsorption energies that $EMIM^+$ adsorbs strongly on TTF-Por COF than TTF-Da COF.

3. Conclusions

This work investigated the charge storage mechanism of donor–acceptor type 2D COFs in various electrolytes like aqueous, organic, and ionic liquid, when operated as EDLC supercapacitor. It was observed in the TTF-based COFs with almost similar surface area and crystallinity, that the charge storage was governed by pore size and surface charge density arising due to different electron acceptor groups. The DFT calculations confirmed that in TTF-Por COFs, $EMIM^+$ could be adsorbed on top of the porphyrin ring by +0.26 eV more strongly than in TTF-Da COF. This allowed a greater overscreening length and a wider EDLC window of TTF-Por COF in $EMIMBF_4$ electrolyte. After pore-confinement, the ionic liquid underwent phase transition to accommodate within the polar micropores, which ultimately led to higher power density as compared to aqueous or organic electrolyte. The EDLC devices exhibited ≈58 Wh kg^{-1} energy density at power density of 1 kW kg^{-1}, which is almost six times higher than in the organic electrolyte. The performances were higher than the commercial activated carbon and comparable to mesoporous carbon EDLC and COF-based pseudocapacitors. However, since no Faradaic reactions were involved, unlike pseudocapacitors, the TTF-COF based devices retained ≈75–88% capacitance after 100 h of usage in ionic liquid electrolyte. The study aimed at improving the understanding of double layer charging mechanism of pore-confined ionic liquid and their effect under the influence of different surface charge densities arising from COF building blocks. Since matching the pore size of nanomaterials and the electrolyte leads to improved capacitance and power density, COFs can further be used to tune the physical properties and provide design guidance for light-weight electrode architectures of future electrical vehicles.

Supporting Information

Supporting Information is available from the Wiley Online Library or from the author.

Acknowledgements

A.C. acknowledges the financial support by the FWO postdoctoral fellowship (12T7521N). J.M.S. acknowledges the financial support from the Ghent University (BOF CSC preference program 01SC0619) and the China Scholarship Council (CSC, 201906060159). K.S.R., V.V.S., and P.V.D.V. acknowledges the financial support by the Research Board of Ghent University (BOF) through a Concerted Research Action (GOA010-17). The computational resources (Stevin Supercomputer Infrastructure) and services used in this work were provided by the VSC (Flemish Supercomputer Center), funded by Ghent University, FWO and the Flemish Government—department EWI.

Conflict of Interest

The authors declare no conflict of interest.

Data Availability Statement

The data that support the findings of this study are available in the supplementary material of this article.

Keywords

covalent organic frameworks, donor–acceptor, electrical double-layer capacitors , ionic liquid, supercapacitors

Received: April 16, 2023
Revised: July 4, 2023
Published online:

[1] N. Jäckel, P. Simon, Y. Gogotsi, V. Presser, *ACS Energy Lett.* **2016**, *1*, 1262.
[2] T. Brousse, D. Bélanger, K. Chiba, M. Egashira, F. Favier, J. Long, J. R. Miller, M. Morita, K. Naoi, P. Simon, W. Sugimoto, in *Springer Handbook of Electrochemical Energy*, Springer, New York **2016**, pp. 495–561.
[3] R. Yan, M. Antonietti, M. Oschatz, *Adv. Energy Mater.* **2018**, *8*, 1800026.
[4] S. Bi, H. Banda, M. Chen, L. Niu, M. Chen, T. Wu, J. Wang, R. Wang, J. Feng, T. Chen, M. Dincă, A. A. Kornyshev, G. Feng, *Nat. Mater.* **2020**, *19*, 552.
[5] H. Shao, K. Xu, Y. C. Wu, A. Iadecola, L. Liu, H. Ma, L. Qu, E. Raymundo-Piñero, J. Zhu, Z. Lin, P. L. Taberna, P. Simon, *ACS Energy Lett.* **2020**, *5*, 2873.
[6] S. Chandra, D. R. Chowdhury, M. Addicoat, T. Heine, A. Paul, R. Banerjee, *Chem. Mater.* **2017**, *29*, 2074.
[7] B. Sun, J. Liu, A. Cao, W. Song, D. Wang, *Chem. Commun.* **2017**, *53*, 6303.
[8] J. Sun, A. Klechikov, C. Moise, M. Prodana, M. Enachescu, A. V. Talyzin, *Angew. Chem., Int. Ed.* **2018**, *57*, 1034.
[9] S. Haldar, D. Rase, P. Shekhar, C. Jain, C. P. Vinod, E. Zhang, L. Shupletsov, S. Kaskel, R. Vaidhyanathan, *Adv. Energy Mater.* **2022**, *12*, 2200754.
[10] R. Kushwaha, S. Haldar, P. Shekhar, A. Krishnan, J. Saha, P. Hui, C. P. Vinod, C. Subramaniam, R. Vaidhyanathan, *Adv. Energy Mater.* **2021**, *11*, 2003626.
[11] Y. Yusran, H. Li, X. Guan, D. Li, L. Tang, M. Xue, Z. Zhuang, Y. Yan, V. Valtchev, S. Qiu, Q. Fang, *Adv. Mater.* **2020**, *32*,1907289.
[12] Z. Gan, Y. Wang, M. Wang, E. Gao, F. Huo, W. Ding, H. He, S. Zhang, *J. Mater. Chem. A* **2021**, *9*, 15985.
[13] Y. Shi, X. Zhao, Q. Liu, Z. Pan, C. Liu, S. Zhu, Z. Zuo, X. Yang, *Green Energy Environ.* **2022**.
[14] Z. Huang, R. Hempelmann, Y. Zhang, L. Tao, R. Chen, *Green Energy Environ.* **2022**.
[15] G. Feng, S. Li, V. Presser, P. T. Cummings, *J. Phys. Chem. Lett.* **2013**, *4*, 3376.
[16] M. Z. Bazant, B. D. Storey, A. A. Kornyshev, *Phys. Rev. Lett.* **2011**, *106*, 6.
[17] R. Futamura, T. Iiyama, Y. Takasaki, Y. Gogotsi, M. J. Biggs, M. Salanne, J. Ségalini, P. Simon, K. Kaneko, Nature Mater. **2017**, *12*, 12.
[18] A. Elbourne, S. McDonald, K. Voïchovsky, F. Endres, G. G. Warr, R. Atkin, *ACS Nano* **2015**, *9*, 7608.
[19] K. Kiyohara, T. Sugino, K. Asaka, *J. Chem. Phys.* **2011**, *134*, 154710.
[20] S.-L. Cai, Y.-B. Zhang, A. B. Pun, B. He, J. Yang, F. M. Toma, I. D. Sharp, O. M. Yaghi, J. Fan, S.-R. Zheng, W.-G. Zhang, Y. Liu, *Chem. Sci.* **2014**, *5*, 4693.
[21] Q. Wu, R. K. Xie, M. J. Mao, G. L. Chai, J. D. Yi, S. S. Zhao, Y. B. Huang, R. Cao, *ACS Appl. Mater. Interfaces* **2020**, *5*,1005.
[22] G. Bian, J. Yin, J. Zhu, *Small* **2021**, *17*, 2006043.
[23] B. Kastening, *Ber. Bunsenges. Phys. Chem.* **1998**, *102*, 229.
[24] H. Yang, M. Yoshio, K. Isono, R. Kuramoto, *Electrochem. Solid-State Lett.* **2002**, *5*, A141.
[25] C. Pei, M. S. Choi, X. Yu, H. Xue, B. Y. Xia, H. S. Park, *J. Mater. Chem. A* **2021**, *9*, 8832.
[26] M. Li, J. Liu, T. Zhang, X. Song, W. Chen, L. Chen, *Small* **2021**, *17*, 2005073.
[27] Q. Shao, J. Tang, Y. Lin, J. Li, F. Qin, K. Zhang, J. Yuan, L.-C. Qin, *Electrochim. Acta* **2015**, *176*, 1441.
[28] T. Romann, O. Oll, P. Pikma, H. Tamme, E. Lust, *Electrochim. Acta* **2014**, *125*, 183.
[29] F. W. Richey, B. Dyatkin, Y. Gogotsi, Y. A. Elabd, *J. Am. Chem. Soc.* **2013**, *135*, 12818.
[30] Y. Shao, J. Li, Y. Li, H. Wang, Q. Zhang, R. B. Kaner, *Mater. Horiz.* **2017**, *4*, 1145.
[31] F. B. Sillars, S. I. Fletcher, M. Mirzaeian, P. J. Hall, *Phys. Chem. Chem. Phys.* **2012**, *14*, 6094.
[32] Y. C. Wu, J. Ye, G. Jiang, K. Ni, N. Shu, P. L. Taberna, Y. Zhu, P. Simon, *Angew. Chem., Int. Ed.* **2021**, *60*, 13317.
[33] J. Ye, Y. C. Wu, K. Xu, K. Ni, N. Shu, P. L. Taberna, Y. Zhu, P. Simon, *J. Am. Chem. Soc.* **2019**, *141*, 16559.
[34] M. D. Stoller, C. W. Magnuson, Y. Zhu, S. Murali, J. W. Suk, R. Piner, R. S. Ruoff, *Energy Environ. Sci.* **2011**, *4*, 4685.
[35] H. Yin, H. Shao, B. Daffos, P. L. Taberna, P. Simon, *Electrochem. Commun.* **2022**, *137*, 107258.
[36] A. Y. Mehandzhiyski, X. Wang, C. Anquetil-Deck, D. Chen, B. A. Grimes, *Energy Mater. Adv.* **2021**, *2021*,9849202.
[37] R. Wen, B. Rahn, O. M. Magnussen, *Angew. Chemie Int, Ed.* **2015**, *54*, 6062.
[38] W. Y. Tsai, P. L. Taberna, P. Simon, *J. Am. Chem. Soc.* **2014**, *136*, 8722.
[39] R. Wen, B. Rahn, O. M. Magnussen, *Angew. Chem.* **2015**, *127*, 6160.
[40] J. P. Perdew, K. Burke, M. Ernzerhof, *Phys. Rev. Lett.* **1996**, *77*, 3865.
[41] S. Grimme, J. Antony, S. Ehrlich, H. Krieg, *J. Chem. Phys.* **2010**, *132*, 154104.
[42] S. Grimme, S. Ehrlich, L. Goerigk, *J. Comput. Chem.* **2011**, *32*, 1456.
[43] G. Kresse, J. Furthmüller, *Comput. Mater. Sci.* **1996**, *6*, 15.
[44] G. Kresse, D. Joubert, *Phys. Rev. B* **1999**, *59*, 1758.